Monthly Notices
of the
ROYAL ASTRONOMICAL SOCIETY

MNRAS **465,** 3483–3494 (2017)
Advance Access publication 2016 November 22

doi:10.1093/mnras/stw2956

Star formation triggered by non-head-on cloud–cloud collisions, and clouds with pre-collision sub-structure

S. K. Balfour,[1]★ A. P. Whitworth[1] and D. A. Hubber[2,3]

[1]*School of Physics and Astronomy, Cardiff University, Cardiff CF24 3AA, Wales, UK*
[2]*University Observatory Munich, Ludwig-Maximilians-University Munich, Scheinerstr.1, D-81679 Munich, Germany*
[3]*Excellence Cluster Universe, Boltzmannstr. 2, D-85748 Garching, Germany*

Accepted 2016 November 14. Received 2016 November 13; in original form 2016 June 11

ABSTRACT

In an earlier paper, we used smoothed particle hydrodynamics (SPH) simulations to explore star formation triggered by head-on collisions between uniform-density 500 $M_\odot$ clouds, and showed that there is a critical collision velocity, $v_{\rm CRIT}$. At collision velocities below $v_{\rm CRIT}$, a hub-and-spoke mode operates and delivers a monolithic cluster with a broad mass function, including massive stars ($M_\star \gtrsim 10\,M_\odot$) formed by competitive accretion. At collision velocities above $v_{\rm CRIT}$, a spider's-web mode operates and delivers a loose distribution of small sub-clusters with a relatively narrow mass function and no massive stars. Here we show that, if the head-on assumption is relaxed, $v_{\rm CRIT}$ is reduced. However, if the uniform-density assumption is also relaxed, the collision velocity becomes somewhat less critical: a low collision velocity is still needed to produce a global hub-and-spoke system and a monolithic cluster, but, even at high velocities, large cores – capable of supporting competitive accretion and thereby producing massive stars – can be produced. We conclude that cloud–cloud collisions may be a viable mechanism for forming massive stars – and we show that this might even be the major channel for forming massive stars in the Galaxy.

Key words: stars: kinematics and dynamics.

1 INTRODUCTION

When two interstellar clouds collide, they may produce dense, gravitationally unstable layers of gas, and thereby trigger star formation. However, it is difficult to evaluate whether cloud–cloud collisions make a significant contribution to the overall galactic star formation rate, since it is difficult to estimate how frequently clouds collide at sufficient speed, or to establish how star formation proceeds when they do (e.g. Pongracic et al. 1992; Chapman et al. 1992; Whitworth et al. 1994; Heitsch et al. 2006; Inoue & Fukui 2013; Dobbs, Pringle & Duarte-Cabral 2015). Moreover, instances where on-going star formation may have been triggered by cloud–cloud collisions are difficult to identify, and the observations are hard to interpret unambiguously (Haworth et al. 2015). Possible examples include Westerlund 2 (Furukawa et al. 2009; Ohama et al. 2010), the Trifid Nebula (Torii et al. 2011) and the Serpens Main Cluster (Duarte-Cabral et al. 2011).

In a previous paper (Balfour et al. 2015, hereafter Paper I), we have simulated head-on collisions between identical uniform-density molecular clouds. We show that such collisions can trigger two rather distinct modes of star formation, depending on whether the collision velocity is less than or greater than a critical value $v_{\rm CRIT} \sim 1.6\,{\rm km\,s^{-1}}$. In both modes, the resulting shock-compressed layer fragments gravitationally into a network of filaments.

At lower collision velocities, $v_{\rm O} < v_{\rm CRIT}$, it takes a longer time for the layer to accumulate sufficient column density to become gravitationally unstable. During this time, the layer starts to collapse laterally, i.e. towards the axis of cylindrical symmetry. This has the effect of dragging and stretching the filaments into spoke-like radial orientations, so that they feed gas and newly formed low-mass stars towards a central hub. A dense cluster forms in the hub, and competitive accretion delivers a significant number of massive stars ($M_\star \gtrsim 10\,M_\odot$). There are also dynamical ejections of stars, of all masses. The overall arrangement of the gas and stars, as projected on the (y, z)-plane, has a hub-and-spoke pattern, and the mass function of the stars formed is relatively broad; we refer to this as the *hub-and-spoke* mode of star formation.

In contrast, at higher velocities, $v_{\rm O} > v_{\rm CRIT}$, the layer accumulates sufficient column density to become gravitationally unstable more rapidly, and there has not been enough time for significant lateral collapse. Consequently, a network of filaments with approximately random orientations develops, and where the filaments intersect, small star-forming cores form. The masses of these cores are limited, because each can only accrete from the few short filamentary sections that are closest to it. Moreover, the cores tend to collapse

★ E-mail: scott.balfour@astro.cf.ac.uk

and fragment independently of one another. This means that each core can only spawn a few stars, and it is rather hard to form massive stars. The overall arrangement of the gas and stars, as projected on the (y, z)-plane, has a spider's-web pattern, and the mass function of the stars is relatively narrow; we refer to this as the *spider's-web* mode of star formation.

However, head-on collisions between uniform-density clouds are an idealization, and we have therefore extended the simulations of Paper I, (i) to non-head-on collisions (i.e. collisions at finite impact parameter, $b_{\rm O}$), and (ii) to pre-collision clouds with internal substructure (i.e. fractal pre-collision clouds). These simulations are reported in the present paper, and the results contrasted with those from Paper I. In Section 2, we describe the numerical method used and the constitutive physics. In Section 3, we present and discuss simulations of *non*-head-on cloud–cloud collisions between uniform-density clouds. In Section 4, we present and discuss simulations of head-on collisions in which the pre-collisions clouds have fractal internal sub-structure. In Section 5, we discuss the results and their limitations. In the Appendix, we estimate the rate at which massive stars form in the Galaxy, as a result of cloud–cloud collisions, and show that this could be a significant contribution to the overall massive star formation rate. Our main conclusions are summarized in Section 6.

2 NUMERICAL METHOD AND CONSTITUTIVE PHYSICS

2.1 Numerical method

The simulations are performed with the smoothed particle hydrodynamics (SPH) code GANDALF (Hubber et al., in preparation). A binary tree is used to compute gravitational forces and collate particle neighbour lists. The grad-h formulation of the evolution equations is invoked (Price & Monaghan 2004), and they are solved with a second-order leapfrog integrator. Artificial viscosity is treated using the method of Monaghan (1997), with parameters $\alpha = 1$ and $\beta = 2$. Sinks are introduced and evolved using the standard procedure described in Hubber, Walch & Whitworth (2013), with $\rho_{\rm SINK} = 10^{-12}\,{\rm g\,cm^{-3}}$; hence condensations which are converted into sinks are already well into their Kelvin–Helmholtz contraction phase, and their properties are essentially independent of the choice of $\rho_{\rm SINK}$.

2.2 Constitutive physics

The gas is evolved with a barotropic equation of state,

$$T(\rho) = T_{\rm O}\left\{1 + \left(\frac{\rho}{\rho_{\rm CRIT}}\right)^{2/3}\right\}, \qquad (1)$$

with $T_{\rm O} = 10\,{\rm K}$ and $\rho_{\rm CRIT} = 10^{-14}\,{\rm g\,cm^{-3}}$. At low densities, $\rho \ll \rho_{\rm CRIT}$, the gas is approximately isothermal at $\sim$10 K. At high densities, $\rho \gg \rho_{\rm CRIT}$, the gas is approximately adiabatic with adiabatic index $\gamma \simeq 5/3$ (corresponding to cool molecular hydrogen in which the rotational degrees of freedom are not significantly excited, plus some monatomic helium). Barotropic prescriptions like equation (1) mimic approximately the variation of temperature with density at the centre of a $1\,{\rm M}_\odot$ protostar (Masunaga & Inutsuka 1999), and have been widely used in simulations of star formation (e.g. Goodwin, Whitworth & Ward-Thompson 2004; Bonnell, Clark & Bate 2008; Bate 2011).

Feedback from stars is not included. As in Paper I, the simulations are simply terminated once 10 per cent of the total mass has been converted into stars, on the assumption that feedback would terminate star formation around this stage. We are presently repeating the simulations discussed here, with ionizing feedback from the most massive stars included, in order to evaluate the consequences for the efficiency of star formation and the stellar mass function. These simulations indicate somewhat higher efficiencies, 10–20 per cent at low collision velocity, $v_{\rm o} \sim 1.2\,{\rm km\,s^{-1}}$, rising to 20–40 per cent at high collision velocity, $v_{\rm o} \sim 2.0\,{\rm km\,s^{-1}}$. These simulations with ionizing feedback also produce very realistic bipolar HII regions (e.g. Deharveng et al. 2015). They will be presented in a future paper.

3 NON-HEAD-ON COLLISIONS BETWEEN UNIFORM-DENSITY CLOUDS

3.1 Initial conditions for non-head-on collisions

3.1.1 *Impact parameter of a non-head-on collision*

If two identical clouds, each with radius $R_{\rm O}$, approach one another from large separation with anti-parallel velocities $\pm v_{\rm O}$, the impact parameter, $b_{\rm O}$, is the distance between the cloud centres, at the point of closest approach, if the clouds velocities are held constant (i.e. we neglect accelerations due to their mutual gravity or hydrodynamic interaction, and they therefore continue in straight lines). Thus, the head-on case corresponds to $b_{\rm O} = 0$. The maximum impact parameter for a collision is

$$b_{\rm MAX} = 2R_{\rm O}\left\{1 + \frac{GM_{\rm O}}{2R_{\rm O}v_{\rm O}^2}\right\}^{1/2}, \qquad (2)$$

corresponding to a glancing collision. The integrated probability of a collision at impact parameter below $b_{\rm O}$ is

$$P(<b_{\rm O}) = \left(\frac{b_{\rm O}}{b_{\rm MAX}}\right)^2, \qquad (3)$$

so the majority of collisions are at large impact parameter.

3.1.2 *Initial configuration for non-head-on collisions*

As in Paper I, both clouds involved in these non-head-on collision initially have mass $M_{\rm O} = 500\,{\rm M}_\odot$, radius $R_{\rm O} = 2\,{\rm pc}$ and uniform density $\rho_{\rm O} = 1.01 \times 10^{-21}\,{\rm g\,cm^{-3}}$ (hence freefall time $t_{\rm FF} = 2.1\,{\rm Myr}$). The impact parameter is introduced in the y-direction, so the cloud centres are initially located at,

$$\boldsymbol{r} \equiv (x, y, z) = (\pm 1.01R_{\rm O}, \pm b_{\rm O}/2, 0)\,, \qquad (4)$$

and the initial velocities are

$$\boldsymbol{v}_{\rm O} = (\mp v_{\rm O}, 0, 0)\,. \qquad (5)$$

We consider two impact parameters, $b_{\rm O} = 0.25\,{\rm pc}\,(=R_{\rm O}/8)$ and $b_{\rm O} = 0.50\,{\rm pc}\,(=R_{\rm O}/4)$. For $b_{\rm O} = 0.25\,{\rm pc}$, we perform a total of 30 simulations, comprising five realizations for each of the six collision velocities $v_{\rm O} = 1.0$, 1.2, 1.4, 1.6, 1.8 and $2.0\,{\rm km\,s^{-1}}$. For $b_{\rm O} = 0.50\,{\rm pc}$, we perform a total of 35 simulations, comprising five realizations for each of the seven collision velocities $v_{\rm O} = 0.8$, 1.0, 1.2, 1.4, 1.6, 1.8 and $2.0\,{\rm km\,s^{-1}}$. The velocity ranges are dictated by the need to bracket the value where the hub-and-spoke mode gives way to the spider's-web mode. The uniform-density clouds are modelled with $\mathcal{N}_{\rm SPH} = 10^6$ SPH particles, so each particle has mass $0.001\,{\rm M}_\odot$, and star formation is resolved down to $\sim 0.05\,{\rm M}_\odot$.

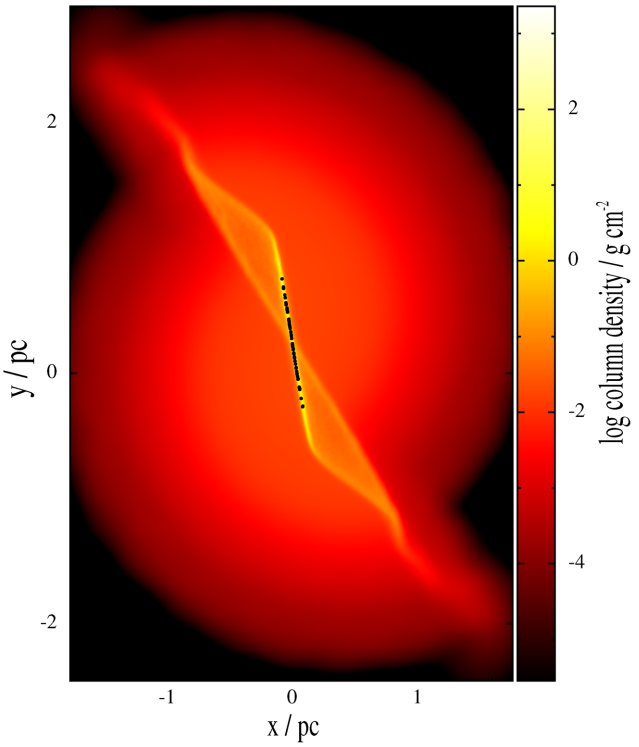

Figure 1. False-colour image at time $t_{10\,\mathrm{per\,cent}} = 1.22\,\mathrm{Myr}$ (i.e. when 10 per cent of the mass has been converted into stars), for a simulation involving uniform-density clouds colliding at impact parameter $b_\mathrm{O} = R_\mathrm{O}/4 = 0.50\,\mathrm{pc}$ and collision velocity $v_\mathrm{O} = 2.0\,\mathrm{km\,s^{-1}}$. Colour represents $\log_{10}\{\Sigma/\mathrm{g\,cm^{-2}}\}$, where Σ is column density projected on the (x,y)-plane. The black dots represent stars.

To create a uniform-density cloud, we position SPH particles randomly in a cubic box. Then we settle them using periodic boundary conditions – with a fixed universal temperature and neglecting gravity – to produce a *glass*. Finally, we cut a sphere from the box. Different realizations are generated by starting with different initial distributions of SPH particles (i.e. using a different random number seed to position the first particle). In the context of SPH, a *glass* means that the density is very close to uniform (typical fractional variations in the density are $\lesssim$0.005) but the particles are not in a regular crystalline array (for example, not in a hexagonal close-packed configuration).

3.2 Results for non-head-on collisions

3.2.1 Overview of non-head-on collisions between uniform-density clouds

When uniform-density clouds collide at finite impact parameter, $b_\mathrm{O} > 0$, the system has bulk angular momentum. This has two consequences. First, the layer tumbles about the z-axis (perpendicular to the page on Fig. 1), because the part of the layer at positive y is dominated by material from the cloud that started at positive x, and therefore has bulk linear momentum in the negative x-direction; conversely the part of the layer at negative y is dominated by material from the cloud that started at negative x, and therefore has bulk linear momentum in the positive x-direction. Second, this means that the layer, and the shocks bounding it, are not perpendicular to the x-axis, and hence not perpendicular to the velocity of the material flowing into the layer. As a result, the material in the layer has a strong shear, with material on either side of the slanting contact discontinuity trying to flow parallel to the contact discontinuity but in opposite directions. This is likely to result in the generation of turbulence. Both these effects (centrifugal acceleration due to the angular momentum, and hydrodynamic support due to the turbulence) slow down the lateral collapse of the layer towards z-axis, and hence it becomes harder to form a hub-and-spoke system. Specifically, the larger the impact parameter of the collision, b_O, the smaller the critical velocity, v_CRIT, below which the hub-and-spoke mode dominates – and thereby generates a broad mass function by fuelling competitive accretion in a large central cluster.

3.2.2 Hydrodynamics for non-head-on collisions between uniform-density clouds

Fig. 1 shows column density, projected on the (x, y)-plane (i.e. looking across the collision axis), for a simulation with impact parameter $b_\mathrm{O} = 0.5\,\mathrm{pc}\,(=R_\mathrm{O}/4)$ and collision velocity $v_\mathrm{O} = 2.0\,\mathrm{km\,s^{-1}}$, at time $t_{10\,\mathrm{per\,cent}} = 1.22\,\mathrm{Myr}$. Because the pre-collision clouds have uniform density, the distribution of gas and stars is very regular. In particular, we focus on the very dense gas in the central sector of the shock-compressed layer, since this is where the stars form. This central sector is the part of the layer where the flux of material from the two clouds is comparable (although not exactly equal), and therefore the column density of the layer builds up rapidly. The layer is tilted relative to the y-axis because it is tumbling about the z-axis (which is directed into the page), due to the bulk angular momentum of the two clouds. In addition, the material in the layer is sheared, with the gas entering from the right (the cloud that started at positive x) tending to flow upwards once it has accreted on to the layer (i.e. towards positive y), and the gas entering from the left (the cloud that started at negative x) tending to flow downwards once it has accreted on to the layer (i.e. towards negative y). These adjacent counter-flowing gas streams are likely to mix, thereby converting some of the kinetic energy of the counterflow into turbulence. The resulting centrifugal acceleration and turbulent velocity dispersion slow down the lateral collapse of the layer (towards the origin). As a result, the filaments that regulate the fragmentation of the layer are dragged and stretched into radial orientations more slowly, and it requires a lower collision velocity, v_O, to have sufficient time to form a global hub-and-spoke system.

This is illustrated in Figs 2 and 3, which show column density, projected on the (y, z)-plane (i.e. looking along the collision axis), at t_{10} per cent, for simulations with – respectively – $b_\mathrm{O} = 0.25\,\mathrm{pc}\,(=R_\mathrm{O}/8)$ and $v_\mathrm{O} = 1.0, 1.2, 1.4, 1.6, 1.8$ and $2.0\,\mathrm{km\,s^{-1}}$, and for simulations with $b_\mathrm{O} = 0.50\,\mathrm{pc}\,(=R_\mathrm{O}/4)$ and $v_\mathrm{O} = 0.8, 1.0, 1.2, 1.4, 1.6$ and $1.8\,\mathrm{km\,s^{-1}}$. The montages show results obtained with the same initial clouds (and hence the same particle noise), but different collision velocities, and the range of velocities has in each case been adjusted to bracket the value where the hub-and-spoke mode gives way to the spider's-web mode. At high collision velocity, v_O, the pattern of fragmentation is very similar to the high collision velocity, head-on case presented in Paper I. A network of filaments forms, and small local cores condense out where the filaments intersect. These small local cores comprise a rather limited reservoir of mass, and therefore they spawn just a few stars, and no massive ones; they complete their collapse and fragmentation more-or-less independently of one another. This is the spider's-web mode of star formation, already identified in Paper I.

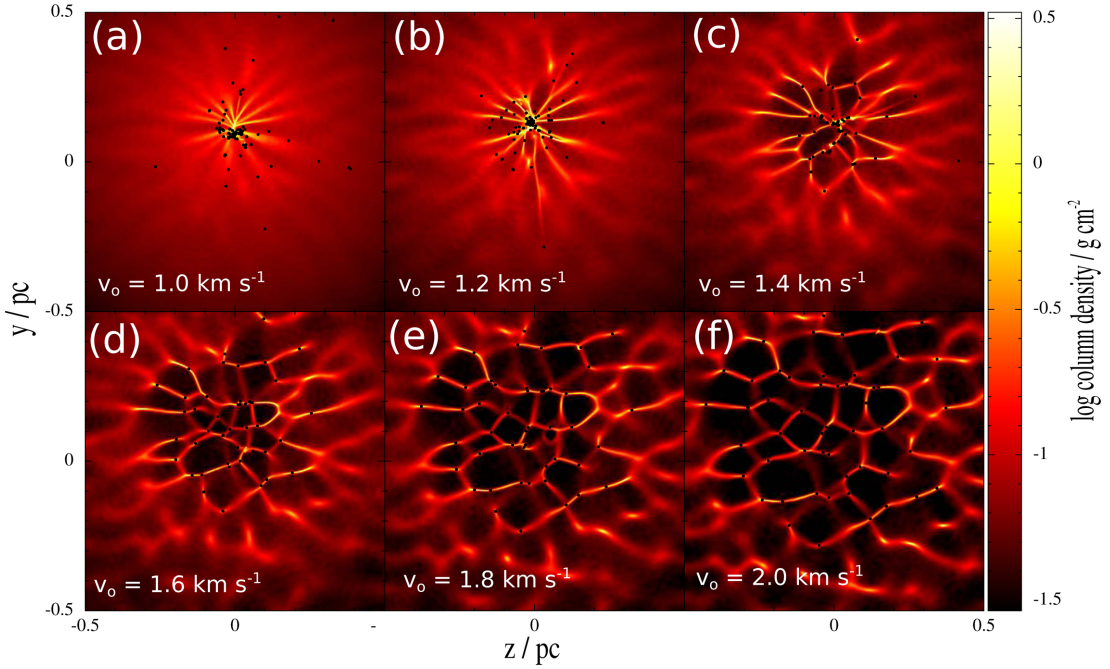

Figure 2. False-colour images at time $t_{10\,\mathrm{per\,cent}}$, for simulations involving uniform-density clouds colliding at impact parameter $b_\mathrm{O} = 0.25\,\mathrm{pc}\,(=R_\mathrm{O}/8)$ and different collision velocities: (a) $(v_\mathrm{O}, t_{10\,\mathrm{per\,cent}}) = (1.0\,\mathrm{km\,s^{-1}}, 1.53\,\mathrm{Myr})$; (b) $(1.2\,\mathrm{km\,s^{-1}}, 1.49\,\mathrm{Myr})$; (c) $(1.4\,\mathrm{km\,s^{-1}}, 1.42\,\mathrm{Myr})$; (d) $(1.6\,\mathrm{km\,s^{-1}}, 1.36\,\mathrm{Myr})$; (e) $(1.8\,\mathrm{km\,s^{-1}}, 1.30\,\mathrm{Myr})$; (f) $(2.0\,\mathrm{km\,s^{-1}}, 1.25\,\mathrm{Myr})$. Colour represents $\log_{10}\{\Sigma/\mathrm{g\,cm^{-2}}\}$, where Σ is column-density projected on the (y, z)-plane, i.e. looking along the collision axis. The black dots represent stars.

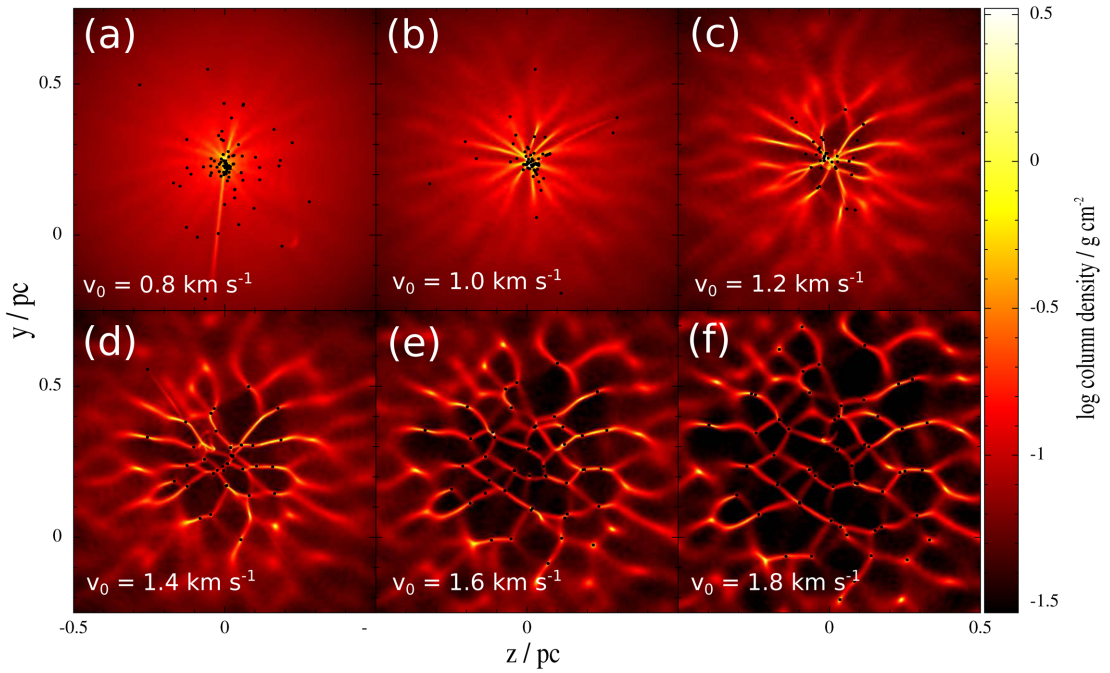

Figure 3. As Fig. 2, but with the larger impact parameter, $b_\mathrm{O} = 0.50\,\mathrm{pc}\,(=R_\mathrm{O}/4)$ and (a) $(v_\mathrm{O}, t_{10\,\mathrm{per\,cent}}) = (0.8\,\mathrm{km\,s^{-1}}, 1.62\,\mathrm{Myr})$; (b) $(1.0\,\mathrm{km\,s^{-1}}, 1.55\,\mathrm{Myr})$; (c) $(1.2\,\mathrm{km\,s^{-1}}, 1.48\,\mathrm{Myr})$; (d) $(1.4\,\mathrm{km\,s^{-1}}, 1.41\,\mathrm{Myr})$; (e) $(1.6\,\mathrm{km\,s^{-1}}, 1.34\,\mathrm{Myr})$; (f) $(1.8\,\mathrm{km\,s^{-1}}, 1.28\,\mathrm{Myr})$.

If the collision velocity, v_O, is reduced, the time required for the column density through the layer to become sufficiently large for the layer to fragment gravitationally increases, and eventually it may become so long that the layer has time to collapse laterally, dragging and stretching the filaments into radial orientations, so that they feed newly formed low-mass stars and residual gas into a central hub, to form a monolithic cluster. As a consequence of the centrifugal acceleration and turbulent velocity dispersion in the layer, the critical collision velocity, v_CRIT (below which this hub-and-spoke mode of star formation operates following a collision between uniform-density clouds), is a decreasing function of the impact parameter of the collision, b_O. Thus, the hub-and-spoke mode requires *both* low collision velocity, v_O, *and* low impact parameter, b_O. From Fig. 2, we see that for $b_\mathrm{O} = 0.25\,\mathrm{pc}\,(=R_\mathrm{O}/8)$ the critical collision velocity

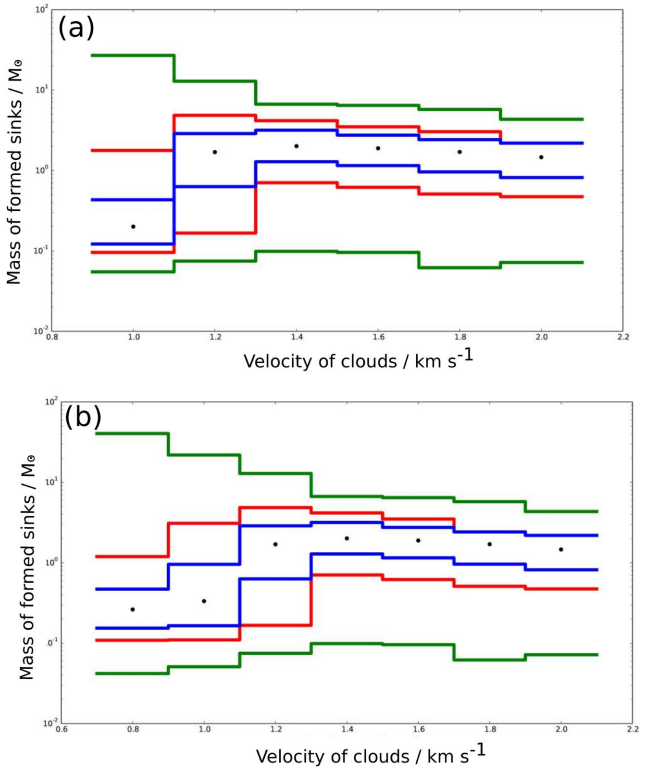

Figure 4. Stellar mass ranges at $t_{10\,\mathrm{per\,cent}}$, for non-head-on collisions of uniform-density pre-collision clouds. (a) $b_\mathrm{O} = 0.25\,\mathrm{pc}$ ($=R_\mathrm{O}/8$) and $v_\mathrm{o} = 1.0, 1.2, 1.4, 1.6, 1.8$ and $2.0\,\mathrm{km\,s^{-1}}$. (b) $b_\mathrm{O} = 0.50\,\mathrm{pc}$ ($=R_\mathrm{O}/4$) and $v_\mathrm{o} = 0.8, 1.0, 1.2, 1.4, 1.6, 1.8$ and $2.0\,\mathrm{km\,s^{-1}}$. For each combination of b_O and v_O, we combine the results from five different realizations. The green lines give the full range of stellar masses, the red lines give the range between the 10th and 90th centiles, the blue lines give the range between the 25th and 75th centiles (the interquartile range) and the filled circles give the *median* mass.

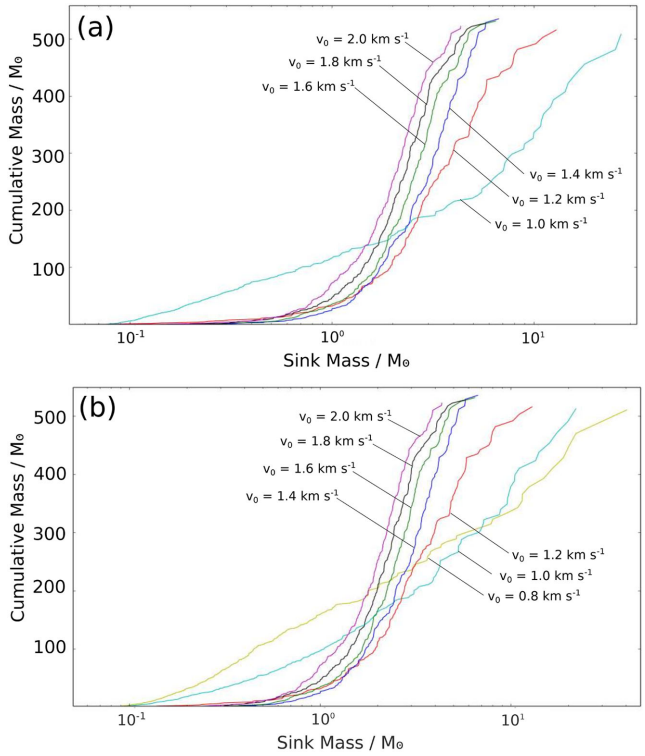

Figure 5. The cumulative mass distribution of the stars at $t_{10\,\mathrm{per\,cent}}$, for non-head-on collisions of uniform-density pre-collision clouds. For each velocity simulated, $v_\mathrm{O} = 0.8\,\mathrm{km\,s^{-1}}$ (yellow curves), $v_\mathrm{O} = 1.0\,\mathrm{km\,s^{-1}}$ (cyan curves), $v_\mathrm{O} = 1.2\,\mathrm{km\,s^{-1}}$ (red curves), $v_\mathrm{O} = 1.4\,\mathrm{km\,s^{-1}}$ (blue curves), $v_\mathrm{O} = 1.6\,\mathrm{km\,s^{-1}}$ (green curves), $v_\mathrm{O} = 1.8\,\mathrm{km\,s^{-1}}$ (black curves) and $v_\mathrm{O} = 2.0\,\mathrm{km\,s^{-1}}$ (purple curves), we combine the results from five different realizations. Panel (a) is for impact parameter $b_\mathrm{O} = 0.25\,\mathrm{pc}$ ($=R_\mathrm{O}/8$). Panel (b) is for $b_\mathrm{O} = 0.50\,\mathrm{pc}$ ($=R_\mathrm{O}/4$).

below which the hub-and-spoke mode operates is of order $v_\mathrm{CRIT} \sim 1.3\,\mathrm{km\,s^{-1}}$. For $b_\mathrm{O} = 0.50\,\mathrm{pc}$ ($=R_\mathrm{O}/4$), it is of order $v_\mathrm{CRIT} \sim 1.1\,\mathrm{km\,s^{-1}}$. In other words, the critical velocity is a function of the impact parameter, $v_\mathrm{CRIT} = v_\mathrm{CRIT}(b_\mathrm{O})$, and $dv_\mathrm{CRIT}/db_\mathrm{O} < 0$.

3.2.3 Stellar mass distribution for non-head-on collisions between uniform-density clouds

These differences between the modes of star formation operating at different collision velocities, v_O, and different impact parameters, b_O, are reflected in the mass functions of the stars that form following a non-head-on collision between uniform-density clouds. In high-velocity collisions, $v_\mathrm{O} > v_\mathrm{CRIT}(b_\mathrm{O})$, the spider's-web mode delivers an array of small local cores, collapsing and fragmenting independently of one another to produce small sub-clusters of stars with quite a narrow range of masses: no massive stars and relatively few very low-mass stars. In low-velocity collisions, $v_\mathrm{O} < v_\mathrm{CRIT}(b_\mathrm{O})$, the hub-and-spoke mode delivers a single, monolithic, central cluster in which a few stars grow too massive by competitive accretion, and there is also a large population of low-mass stars that fall through the centre at high speed and therefore do not accrete much more mass. Consequently, the mass function is significantly broader. This is illustrated in Figs 4 and 5.

Fig. 4 presents the range of stellar masses obtained with the different impact parameters $b_\mathrm{O} = 0.25\,\mathrm{pc}$ (panel a) and $b_\mathrm{O} = 0.50\,\mathrm{pc}$ (panel b), and different collision velocities, v_O. Similarly to the case of head-on collisions between uniform-density clouds (treated in Paper I), as we move from high velocity (the spider's-web mode) to low velocity (the hub-and-spoke mode), the range of masses increases, and hence the most massive stars are more massive, but the median mass decreases, due to the increasing number of very low-mass stars. For $b_\mathrm{O} = 0.25\,\mathrm{pc}$, the switch from spider's-web mode to hub-and-spoke mode occurs at $v_\mathrm{CRIT} \sim 1.3\,\mathrm{km\,s^{-1}}$. For $b_\mathrm{O} = 0.50\,\mathrm{pc}$, the switch occurs at $v_\mathrm{CRIT} \sim 1.1\,\mathrm{km\,s^{-1}}$.

Fig. 5 presents the corresponding cumulative mass plots, to emphasize that these trends are quite regular (given the relatively small-number statistics), with only low-velocity collisions at low impact parameter producing *either* any massive stars, *or* a large population of low-mass stars.

4 PRE-COLLISION CLOUDS WITH SUB-STRUCTURE COLLIDING HEAD-ON

4.1 Initial conditions for pre-collision clouds with sub-structure

4.1.1 Fractal pre-collision density sub-structure

Molecular clouds are very clumpy, and this clumpiness is likely to play an important role in star formation. In Paper I, we invoked pre-collision clouds with uniform density, so that we could isolate the effects of the collision from those that might result from internal

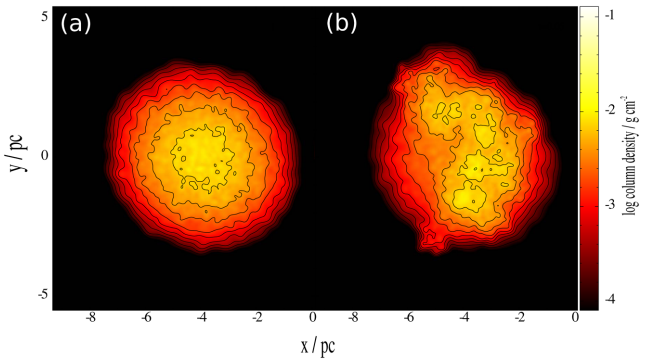

Figure 6. False-colour images of pre-collision clouds with sub-structure. Colour represents $\log_{10}\{\Sigma/\mathrm{g\,cm^{-2}}\}$, where Σ is column density. Panel (a) is a cloud with $\chi = 0$, i.e. mildly clumpy pre-collision sub-structure. Panel (b) is a cloud with $\chi = 8$, i.e. strongly clumpy sub-structure. Contours have been added at $\log_{10}\{\Sigma/\mathrm{g\,cm^{-2}}\} = -2.0$, -2.2, -2.4, -2.6, -2.8, -3.0, -3.2 and $-3.4\,\mathrm{g\,cm^{-2}}$, to emphasize the difference between $\chi = 0$ and $\chi = 8$.

sub-structure in the pre-collision clouds. Here, we explore how adding fractal sub-structure to the pre-collision clouds affects the star formation triggered by a head-on cloud–cloud collision.

The fractal density sub-structure in the pre-collision clouds is created using the method of Whitworth (in preparation), which builds a nested hierarchy of clumps within clumps. The hierarchy is characterized by its fractal dimension, $D_3 = 2.31$ (which determines the extent to which the clumps on one level of the hierarchy fill the volume occupied by the larger clumps on the level above), and its density scaling exponent,

$$\chi = -\frac{\mathrm{d}\ln(\Delta\rho(L))}{\mathrm{d}\ln(L)}\,; \tag{6}$$

here $\Delta\rho(L)$ is the excess density in a clump of linear size L, relative to the background defined by the larger clumps on higher levels of the hierarchy, within which it is nested. We treat two cases: $\chi = 0$ (which gives pre-collision clouds that are *mildly clumpy*, and not hugely different from the uniform-density clouds treated in Paper I) and $\chi = 8$ (which gives pre-collision clouds that are *strongly clumpy* and markedly different from the uniform-density clouds treated in Paper I). Examples of clouds created in this way, one with $\chi = 0$, and one with $\chi = 8$, are shown in Fig. 6.

4.1.2 Initial collision configuration for clouds with sub-structure

The clouds in the simulations presented here have the same mass, $M_0 = 500\,\mathrm{M_\odot}$, as those in Paper I, but we have doubled the initial cloud radius to $R_\mathrm{O} = 4\,\mathrm{pc}$, and so the mean density is $\bar{\rho} = 1.26 \times 10^{-22}\,\mathrm{g\,cm^{-3}}$ (and the mean freefall time is 5.9 Myr). We make this adjustment because otherwise, with density sub-structure added (see below), the densest regions of the pre-collision clouds collapse to form stars before they are involved in the cloud–cloud collision.

The cloud centres are initially located at

$$\boldsymbol{r} \equiv (x, y, z) = (\pm 1.01 R_\mathrm{O}, 0, 0)\,, \tag{7}$$

and the initial velocities are

$$\boldsymbol{v}_\mathrm{O} = (\mp v_\mathrm{O}, 0, 0)\,. \tag{8}$$

We perform a total of 20 simulations using pre-collision clouds with fractal density sub-structure, five realizations for each combination of the two possible fractal density substructures (mildly clumpy, i.e. $\chi = 1$, and strongly clumpy, i.e. $\chi = 8$) and the two extreme collision velocities $v_\mathrm{O} = 1.2$ and $2.0\,\mathrm{km\,s^{-1}}$.

4.1.3 Resolution for clouds with sub-structure

In these simulations (where the pre-collision clouds have fractal sub-structure), we use $\mathcal{N}_\mathrm{SPH} = 10^5$ SPH particles, and so each SPH particle has mass $M_\mathrm{SPH} = 0.01\,\mathrm{M_\odot}$. Consequently, the mass resolution is 10 times lower than in Paper I and in the non-head-on collisions reported in the previous section (where $\mathcal{N}_\mathrm{SPH} = 10^6$ and $M_\mathrm{SPH} = 0.001\,\mathrm{M_\odot}$). This means that, for the simulations involving pre-collision clouds with sub-structure, we cannot resolve stars much below $\sim 0.5\,\mathrm{M_\odot}$. The reduced mass resolution is dictated by the limits of computational resources (there is a bigger spread in the times when the stars form, and therefore the simulations are computationally more demanding) and the need to do multiple realizations (in order to improve statistics). We have therefore repeated the corresponding uniform-density simulations from Paper I, with this reduced resolution, *and* with the increased initial cloud radius (4 pc instead of 2 pc), in order to have a more relevant reference point against which to compare the results obtained here with sub-structure.

4.2 Results for head-on collisions involving clouds with pre-collision sub-structure

4.2.1 Overview of head-on collisions involving clouds with pre-collision sub-structure

Sub-structure in the pre-collision clouds reduces the homogeneity and spatial coherence of the resulting shock compressed layer. In some places, there are large differences between the fluxes of material impinging on opposite sides of the layer, and these differences have a range of length-scales, reflecting the spectrum of spatial frequencies in the intrinsic fractal density fields of the pre-collision clouds. Thus, at some positions, the fluxes from the two sides of the layer may be comparable, producing locally a section of layer close to the (y, z)-plane. However, at other nearby positions, the fluxes from the two sides of the layer may be very different, where a dense clump in one cloud comes up against a much more rarefied region in the other cloud, and in this case the shocked gas has a bulk velocity relative to the (y, z)-plane, and the layer bulges out. Moreover, where the combined fluxes from both sides are larger than average, the column density will buildup more quickly, collapse and fragmentation will occur sooner, and stars will form earlier. Conversely, where the fluxes are smaller than average, the column density will buildup more slowly, collapse and fragmentation will occur later, and stars will form later. (In fact, if feedback is taken into account, these late stars may not form at all.) These effects are inevitably more marked when the pre-collision sub-structure has large amplitude, i.e. in the strongly clumpy case with large density-scaling exponent, $\chi = 8$.

The main consequence of sub-structure in the pre-collision clouds is to blur the distinction between the spider's-web and hub-and-spoke modes of star formation. Both modes still operate, but for a wide range of initial conditions they can occur simultaneously in different parts of the layer. Even at high collision velocity, and even with mildly clumpy sub-structure, there is no longer a semi-periodic spider's web with many comparable cores collapsing and fragmenting, more or less independently and simultaneously. Instead, there are patches on the layer that give the appearance of a spider's web, and other patches that are more like local hubs. Specifically, where the chance confluence of two denser-than-average clumps

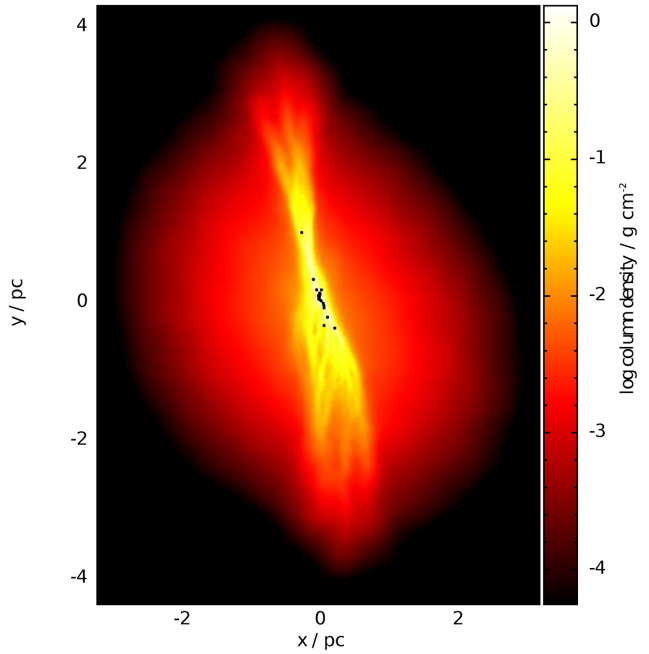

Figure 7. False-colour image at time $t_{10\,\mathrm{per\,cent}} = 2.25$ Myr, for a simulation involving clouds with strongly clumpy ($\chi = 8$) pre-collision sub-structure, colliding head-on ($b_\mathrm{O} = 0$) at collision velocity $v_\mathrm{O} = 1.2\,\mathrm{km\,s^{-1}}$. Colour represents $\log_{10}\{\Sigma/\mathrm{g\,cm^{-2}}\}$, where Σ is column density projected on the (x, y)-plane (i.e. looking across the collision axis). The black dots represent stars.

(one from each cloud) produces a patch on the layer with higher than average column density, this patch fragments into filaments and cores sooner than neighbouring bits of the layer, and starts to pull in additional material from these neighbouring bits and thereby become more massive. If these neighbouring bits of the layer later acquire sufficient column density to fragment into filaments and cores themselves, these filaments may find they are being dragged into the massive cores that formed earlier, thereby producing a local hub-and-spoke system that is sufficiently massive to spawn massive stars by competitive accretion. Otherwise they form a local patch of spider's web, but typically less extensive and less periodic (than those formed in high-velocity collisions of uniform-density clouds).

4.2.2 Hydrodynamics for head-on collisions involving clouds with pre-collision sub-structure

Fig. 7 shows column density, projected on the (x, y)-plane (i.e. looking across the collision axis), at time $t_{10\,\mathrm{per\,cent}} = 2.25$ Myr, for a simulation involving clouds with strongly clumpy pre-collision substructure ($\chi = 8$), colliding head-on ($b_\mathrm{O} = 0$), at collision velocity $v_\mathrm{O} = 1.2\,\mathrm{km\,s^{-1}}$. The distribution of gas and stars is quite irregular. In particular, the layer is broader than for the cases with uniform-density pre-collision clouds. Furthermore, even though this is a head-on collision, the layer is not well aligned with the (y, z)-plane. It is broader because different parts of the layer are displaced parallel to the x-axis, due to local mismatches between the fluxes of material impinging on the two sides of the layer. It is tilted relative to the (y, z)-plane because, in this particular case, due to the stochastic fractal sub-structure in the pre-collision clouds, the centre of mass of the cloud coming from negative x is displaced downwards (to negative y), and the centre of mass of the cloud coming from positive x is displaced upwards (to positive y).

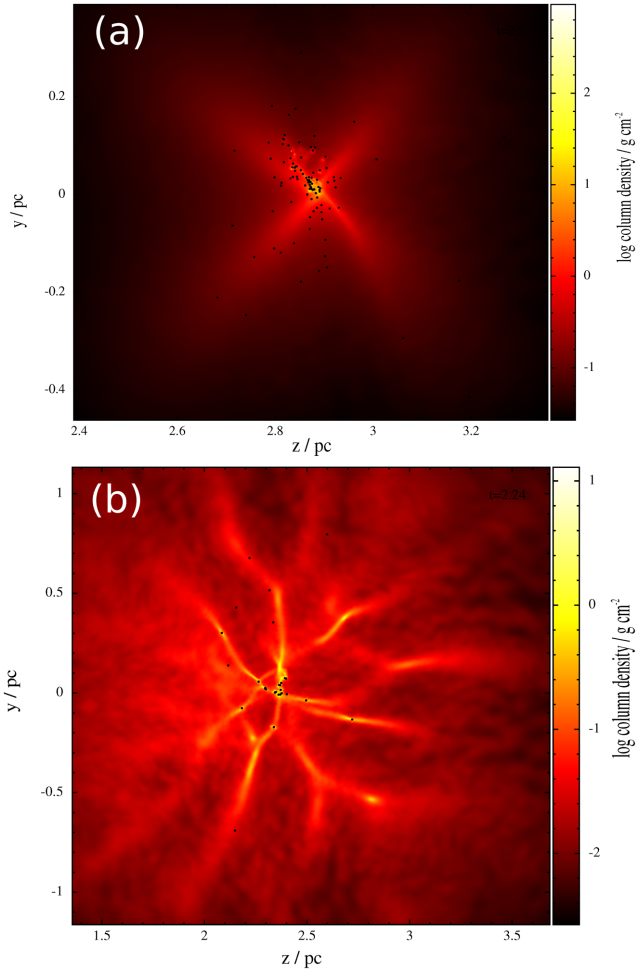

Figure 8. False-colour images at time $t_{10\,\mathrm{per\,cent}}$, for simulations involving clouds with mildly clumpy pre-collision sub-structure ($\chi = 0$), colliding head-on ($b_\mathrm{O} = 0$). In panel (a), the collision velocity is $v_\mathrm{O} = 1.2\,\mathrm{km\,s^{-1}}$ and $t_{10\,\mathrm{per\,cent}} = 2.80$ Myr. In panel (b), $v_\mathrm{O} = 2.0\,\mathrm{km\,s^{-1}}$ and $t_{10\,\mathrm{per\,cent}} = 2.24$ Myr. Colour represents $\log_{10}\{\Sigma/\mathrm{g\,cm^{-2}}\}$, where Σ is column density projected on the (y, z)-plane, i.e. looking along the direction of the collision. The black dots represent stars.

Figs 8 and 9 show column density, projected on the (y, z)-plane (i.e. looking along the collision axis), at $t_{10\,\mathrm{per\,cent}}$, for simulations in which the clouds collide head-on and have, respectively, mildly ($\chi = 0$) and strongly ($\chi = 8$) clumpy pre-collision sub-structure. In the upper panels (a), the clouds collide at collision velocity $v_\mathrm{O} = 1.2\,\mathrm{km\,s^{-1}}$. In the lower panels (b), they collide at $v_\mathrm{O} = 2.0\,\mathrm{km\,s^{-1}}$.

Fig. 8(a) shows the distribution of gas and stars for the head-on collision involving mildly clumpy pre-collision sub-structure ($\chi = 0$) and a relatively low collision velocity ($v_\mathrm{O} = 1.2\,\mathrm{km\,s^{-1}}$). Like the equivalent simulations with uniform-density clouds (see Paper I), this produces a hub-and-spoke arrangement of gas, that feeds a central cluster in which massive stars form by competitive accretion. However, in the simulations presented here (involving clouds with mildly clumpy pre-collision sub-structure), there are fewer filaments feeding the central cluster (just four), and the star formation takes place over a longer period of time (because the layer is more inhomogeneous), so by $t_{10\,\mathrm{per\,cent}}$ the cluster is less centrally condensed. Both these features might make this a better model to reproduce the hub-and-spoke system, SDC335, reported by Peretto et al. (2013).

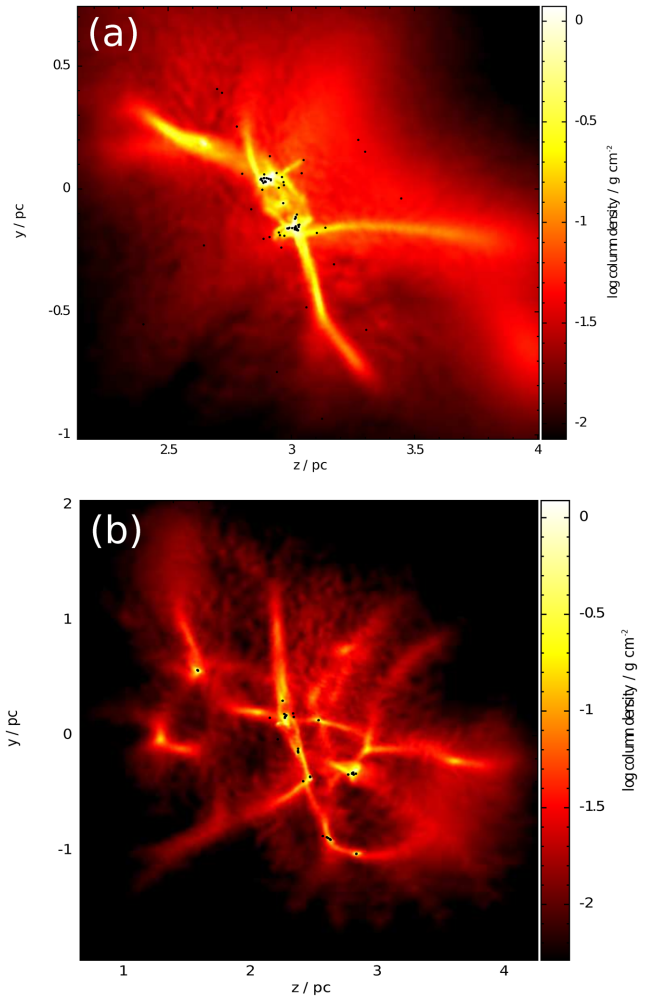

Figure 9. As for Fig. 8, but the pre-collision clouds have strongly clumpy sub-structure ($\chi = 8$), and the times are $t_{10\,\mathrm{per\,cent}} = 2.93$ Myr for collision velocity $v_\mathrm{O} = 1.2\,\mathrm{km\,s^{-1}}$ (panel a), and $t_{10\,\mathrm{per\,cent}} = 2.39$ Myr for $v_\mathrm{O} = 2.0\,\mathrm{km\,s^{-1}}$ (panel b).

Fig. 8(b) shows an example of the distribution of gas and stars following a head-on collision involving mildly clumpy pre-collision sub-structure ($\chi = 0$) and a relatively high collision velocity ($v_\mathrm{O} = 2.0\,\mathrm{km\,s^{-1}}$). Although the gas distribution has some features like a spider's web, by $t_{10\,\mathrm{per\,cent}}$ many of the stars are no longer concentrated in the individual cores where they formed. Again, this is because, due to the non-uniformity of the layer, star formation takes place over a longer period of time (than in the equivalent simulation with uniform-density pre-collision clouds; see Paper I), and therefore many of the stars have had time to fall towards the centre and produce a loose cluster.

Fig. 9(a) shows an example of the distribution of gas and stars following a head-on collision involving strongly clumpy pre-collision sub-structure ($\chi = 8$) and a relatively low collision velocity ($v_\mathrm{O} = 1.2\,\mathrm{km\,s^{-1}}$). The outcome is now completely different from the equivalent simulation with uniform-density clouds (see Paper I). The star formation is dominated by two large dense clusters, which both contain massive stars, and the gas has filamentary structure but there is no hub-and-spoke geometry.

Fig. 9(b) shows an example of the distribution of gas and stars following a head-on collision involving strongly clumpy pre-collision sub-structure ($\chi = 8$) and a relatively high collision velocity ($v_\mathrm{O} = 2.0\,\mathrm{km\,s^{-1}}$). Here, there is a network of relatively isolated cores, independently spawning sub-clusters. However, because the network is much more irregular than in the equivalent simulation involving uniform-density pre-collision clouds (see Paper I), some of the sub-clusters are quite massive and spawn massive stars.

4.2.3 *Stellar mass distribution for head-on collisions involving clouds with pre-collision sub-structure*

Fig. 10 presents the range of stellar masses obtained when clouds with pre-collision sub-structure collide head-on. In panel (a), the pre-collision sub-structure is mildly clumpy ($\chi = 0$), and in panel (b), it is strongly clumpy ($\chi = 8$). In both panels, we consider only two collision velocities $v_\mathrm{O} = 1.2$ and $2.0\,\mathrm{km\,s^{-1}}$. In all cases, we combine data from five different realizations.

For the clouds with mildly clumpy pre-collision sub-structure ($\chi = 0$, Fig. 10a), the median mass increases considerably going from collision velocity $v_\mathrm{O} = 1.2$ to $2.0\,\mathrm{km\,s^{-1}}$, due to a huge decrease in the proportion of very low-mass stars; this is similar to what happens with uniform-density pre-collision clouds (see Paper I). Going from $v_\mathrm{O} = 1.2$ to $2.0\,\mathrm{km\,s^{-1}}$, there is also a decrease in the number of massive stars, but this is less marked than for the uniform-density pre-collision clouds (see Paper I).

For the clouds with strongly clumpy pre-collision sub-structure ($\chi = 8$, Fig. 10b), the same trends are observed, but they are much weaker. Thus, the effect of strongly clumpy pre-collision sub-structure is to blur the distinction between the hub-and-spoke mode of star formation and the spider's-web mode. In particular, at high collision velocity, $v_\mathrm{O} = 2.0\,\mathrm{km\,s^{-1}}$, star formation still occurs in a network of cores, but these cores have a range of masses, and form over an extended period of time, with the result that some of them can spawn massive stars.

Fig. 11 presents the corresponding cumulative mass plots, to emphasize that these trends are quite regular. For the clouds with mildly clumpy pre-collision sub-structure ($\chi = 0$, Fig. 11a), the low collision velocity ($v_\mathrm{O} = 1.2\,\mathrm{km\,s^{-1}}$, red curve) delivers many more very low-mass stars, and somewhat more massive stars, than the high collision velocity ($v_\mathrm{O} = 2.0\,\mathrm{km\,s^{-1}}$, purple curve). For the clouds with strongly clumpy pre-collision sub-structure ($\chi = 8$, Fig. 11b), the same trends are visible, but they are less emphatic.

5 DISCUSSION

We have only considered clouds of a single mass (500 $\mathrm{M}_\odot$), in order to explore, in a systematic way, the effects of other parameters, in particular, collision velocity, impact parameter and level of substructure in the pre-collision clouds. In each case, we have performed multiple realizations, in order to improve the statistics of the resulting stellar masses, and determine robustly any systematic trends. 500 $\mathrm{M}_\odot$ is chosen so as to be large enough to form a range of stellar masses, but at the same time small enough that we can perform multiple simulations while at the same time maintaining good mass resolution. We have not simulated non-head-on collisions of clouds with pre-collision sub-structure, and there are many other parameters that need to be explored, for example, different cloud masses, unequal cloud masses, non-spherical and/or spinning clouds. However, the basic phenomenology explored here appears to offer a credible mechanism for forming star clusters, and, in addition, it suggests three independent circumstances that all promote a broad mass function, and hence the formation of massive stars:

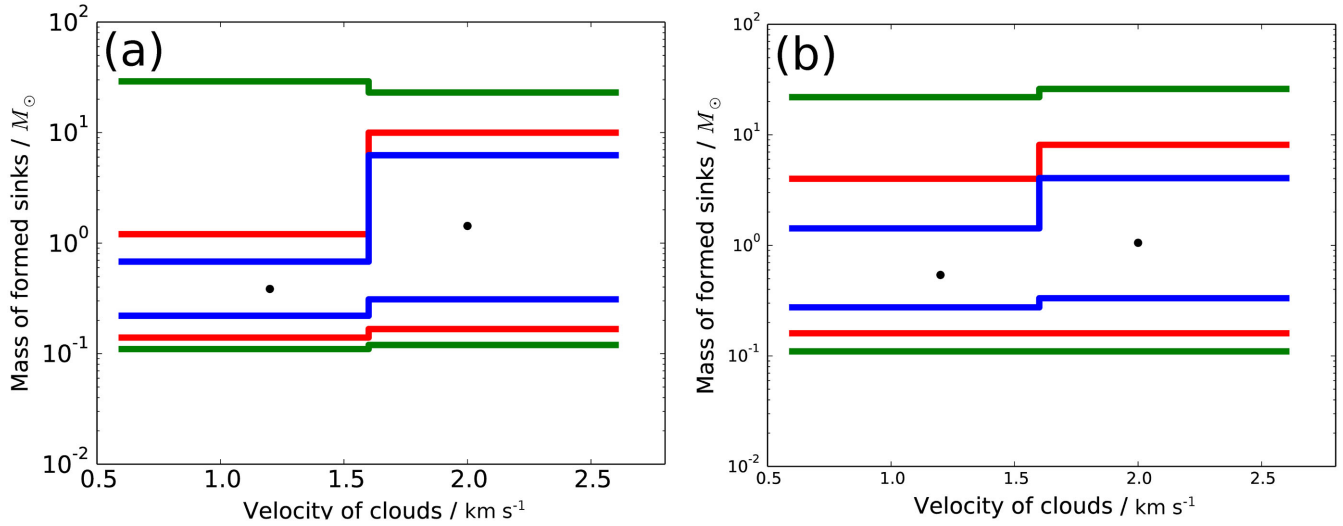

Figure 10. Stellar mass ranges at $t_{10\,\mathrm{per\,cent}}$, for clouds with pre-collision density sub-structure colliding head-on. Panel (a) is for mildly clumpy sub-structure ($\chi = 0$). Panel (b) is for strongly clumpy sub-structure ($\chi = 8$). In each panel, we show results obtained with collision velocities $v_\mathrm{O} = 1.2$ and $2.0\,\mathrm{km\,s^{-1}}$. For each parameter set, (χ, v_O), we have combined the results from five realizations. The green lines give the full range of stellar masses, the red lines give the range between the 10th and 90th centiles, the blue lines give the range between the 25th and 75th centiles (the interquartile range), and the filled circles give the median mass.

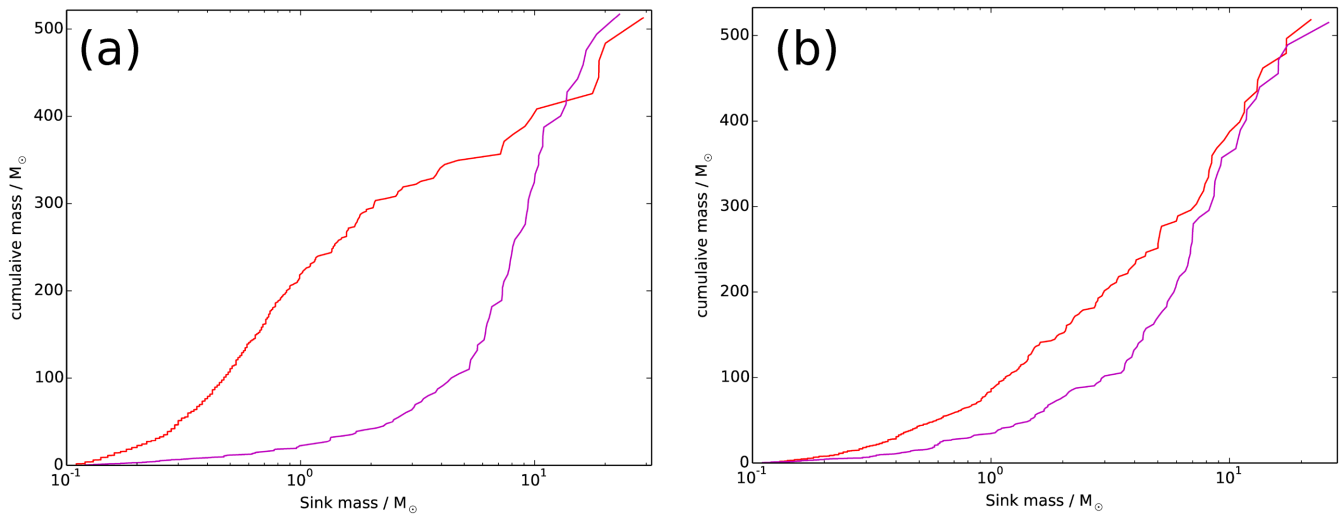

Figure 11. The cumulative mass distribution of the stars at $t_{10\,\mathrm{per\,cent}}$, for clouds with pre-collision density sub-structure colliding head-on. Panel (a) is for mildly clumpy sub-structure ($\chi = 0$). Panel (b) is for strongly clumpy sub-structure ($\chi = 8$). In both panels, the red curve corresponds to collision velocity $v_\mathrm{O} = 1.2\,\mathrm{km\,s^{-1}}$ and the purple curve to $v_\mathrm{O} = 2.0\,\mathrm{km\,s^{-1}}$. In all cases, the curves are obtained by combining five different realizations.

low collision velocity, small impact parameter and pre-collision substructure.

(i) A low collision velocity means that it takes a long time for the layer to buildup sufficient surface density to fragment. This in turn means that there is time for the layer to contract laterally, thereby dragging filaments into radial orientations, so that they feed matter into the central region, feeding a monolithic star cluster in which competitive accretion can operate. Thus, slow collisions promote a broad mass function and the formation of massive stars.

(ii) A *larger* impact parameter means that a smaller fraction of the cloud mass is shock-compressed into a layer. In addition, the mass which is compressed inherits more shear from the bulk angular momentum of the collision, and this probably generates significant turbulent motions in the layer. The large shear (and/or high turbulent velocity dispersion) means that lateral contraction of the layer is slowed, and hence the layer has more time to fragment into many, relatively isolated cores, which are individually too small to form massive stars. Thus, a low impact parameter collision is required to promote a broad mass function and the formation of massive stars.

(iii) Pre-collision sub-structure influences the scales on which the layer fragments, and hence the masses of the cores that form. Instead of the layer accumulating mass until it becomes gravitationally unstable on a length-scale determined simply by its surface density and its internal velocity dispersion, the layer can fragment on scales determined more by the scale of the pre-collision sub-structure – for example where a big lump from one cloud hits a big lump from the other. As long as the pre-collision sub-structure includes large scales, this will promote the formation of massive cores – more massive than for uniform-density pre-collision

clouds – and hence a broad mass function and the formation of massive stars.

If cloud–cloud collisions are a viable mechanism for triggering the formation of massive stars, we should consider whether they might be the dominant mechanism. This requires us to estimate the rate of massive star formation in the Galaxy, due to cloud–cloud collisions, and compare it with estimates of the net rate. Because the former estimate is necessarily compromised by many questionable assumptions and uncertainties, we relegate it to an Appendix. However, modulo these caveats, our estimate of the rate due to cloud–cloud collisions, $\mathcal{R}_{\rm MSF}^{\rm CCC} \simeq 2 \times 10^{-4}\,{\rm Myr}^{-1}$, is comparable with the overall estimate, $\mathcal{R}_{\rm MSF}^{\rm TOT} \simeq 10^{-4}\,{\rm Myr}^{-1}$, suggesting that cloud–cloud collisions might be a major contributor to the overall formation rate of massive stars.

6 CONCLUSIONS

We have extended our exploration of star formation triggered by cloud–cloud collisions to include the effects of finite impact parameter (i.e. clouds not colliding head-on), and the effects of pre-collision sub-structure in the colliding clouds (using a fractal prescription). Our main conclusions are as follows.

(i) When two uniform-density clouds collide at finite impact parameter, the amount of mass that is compressed is reduced (relative to the head-on case), *and* the bulk angular momentum in the collision delivers shear to the shock-compressed gas (which in turn may decay into turbulence) and this gives the layer extra support against lateral contraction. Consequently, the critical collision velocity – below which the filaments condensing out of the layer are dragged and stretched into radial spokes feeding matter into a central monolithic cluster and forming massive stars by competitive accretion – is reduced.

(ii) When the clouds have pre-collision substructure, the collision velocity becomes less critical. Low-velocity collisions are still the most effective at forming massive stars, but even at high collision velocity there are more massive cores, due to the variance in the flux of matter impinging on different parts of the layer. In other words, where occasionally a sufficiently large lump in one cloud runs into a sufficiently large lump in the other, a large core is formed in which competitive accretion can spawn a broad mass function with some massive stars.

(iii) Cloud–cloud collisions appear to be an effective channel for forming massive stars ($M_\star \gtrsim 10\,{\rm M}_\odot$). The collisions that produce massive stars tend to be the slow collisions, at low impact parameter, involving clouds with pre-collision sub-structure.

(iv) Our estimate of the contribution of cloud–cloud collisions to the rate of massive star formation in the Galaxy, $\mathcal{R}_{\rm MSF}^{\rm CCC} \simeq 2 \times 10^{-4}\,{\rm Myr}^{-1}$; see the Appendix) suggests that they might be the dominant mechanism for forming massive stars.

ACKNOWLEDGEMENTS

SKB gratefully acknowledges the support of a PhD studentship, and APW the support of a consolidated grant (ST/K00926/1), from the UK Science and Technology Funding Council. DAH acknowledges the support of the DFG cluster of excellence 'Origin and Structure of the Universe'. This work was performed using the computational facilities of the Advanced Research Computing at Cardiff (ARCCA) Division, Cardiff University. All false-colour images have been rendered with SPLASH (Price 2007).

REFERENCES

Balfour S. K., Whitworth A. P., Hubber D. A., Jaffa S. E., 2015, MNRAS, 453, 2471 (Paper I)
Bate M. R., 2011, MNRAS, 417, 2036
Bonnell I. A., Clark P., Bate M. R., 2008, MNRAS, 389, 1556
Chapman S., Pongracic H., Disney M., Nelson A., Turner J., Whitworth A., 1992, Nature, 359, 207
Deharveng L. et al., 2015, A&A, 582, A1
Dobbs C. L., Pringle J. E., Duarte-Cabral A., 2015, MNRAS, 446, 3608
Duarte-Cabral A., Dobbs C. L., Peretto N., Fuller G. A., 2011, A&A, 528, A50
Furukawa N., Dawson J. R., Ohama A., Kawamura A., Mizuno N., Onishi T., Fukui Y., 2009, ApJ, 696, L115
Goodwin S. P., Whitworth A. P., Ward-Thompson D., 2004, A&A, 423, 169
Haworth T. J. et al., 2015, MNRAS, 450, 10
Heitsch F., Slyz A. D., Devriendt J. E. G., Hartmann L. W., Burkert A., 2006, ApJ, 648, 1052
Hubber D. A., Walch S., Whitworth A. P., 2013, MNRAS, 430, 3261
Inoue T., Fukui Y., 2013, ApJ, 774, L31
Masunaga H., Inutsuka S.-i., 1999, ApJ, 510, 822
Monaghan J. J., 1997, J. Comput. Phys., 136, 298
Ohama A. et al., 2010, ApJ, 709, 975
Peretto N. et al., 2013, A&A, 555, A112
Pongracic H., Chapman S. J., Davies J. R., Disney M. J., Nelson A. H., Whitworth A. P., 1992, MNRAS, 256, 291
Price D. J., 2007, PASA, 24, 159
Price D. J., Monaghan J. J., 2004, MNRAS, 348, 139
Torii K. et al., 2011, ApJ, 738, 46
Whitworth A. P., Bhattal A. S., Chapman S. J., Disney M. J., Turner J. A., 1994, MNRAS, 268, 291

APPENDIX: CAN CLOUD–CLOUD COLLISIONS MAKE A SIGNIFICANT CONTRIBUTION TO THE FORMATION OF MASSIVE STARS?

To estimate the rate at which massive stars (i.e. stars with $M_\star > 10\,{\rm M}_\odot$ that evolve to become supernovae) might form as a consequence of cloud/cloud collisions, in the Galaxy as a whole, we need to make a number of assumptions. We list these assumptions here, along with the default values that we invoke for their coefficients and exponents. For ease of reference, these coefficients and exponents are also listed in Table A1. Where these default values are substituted, to obtain an explicit estimate, we indicate this with the $\rightarrow$ symbol [e.g. equation (A1)].

Assumption 1: The cloud ensemble. We assume that in the Galaxy, star-forming clouds are concentrated in a star-forming disc with radius $R_{\rm MW} \simeq 8\,{\rm kpc}$, and thickness $\Delta Z_{\rm MW} \simeq 0.1\,{\rm kpc}$, hence total volume

$$V_{\rm TOT} \simeq \pi\, R_{\rm MW}^2\, \Delta Z_{\rm MW} \;\rightarrow\; 20\,{\rm kpc}^3\,. \qquad ({\rm A1})$$

Within this star-forming disc, the mass-differential number density of potential colliding clouds (hereafter simply 'clouds') is assumed to approximate to

$$\frac{{\rm d}n}{{\rm d}M} \simeq K_{\rm O} \left(\frac{M}{{\rm M}_\odot}\right)^{\alpha}, M_{\rm MIN} \lesssim M \lesssim M_{\rm MAX}, \qquad ({\rm A2})$$

Table A1. This table contains all the independent parameters (coefficients and exponents) that we define in this appendix, and the default values adopted to estimate the net rate of formation of massive stars in the Galaxy. Values for all other quantities [for example, the fractal dimension, equation (A10)] are derived from these parameters. (The scaling relations, equations (A7) and (A8), give cloud radius and internal velocity dispersion, in terms of cloud mass in units of $\mathrm{M}_\odot$, and therefore we refer to the corresponding coefficients as the radius and internal velocity dispersion of a notional '$\mathrm{M}_\odot$ cloud'. Although these relations are not applied here to such low-mass clouds, they are probably still valid approximations down to $\sim\mathrm{M}_\odot$.)

Parameter	Symbol	Default
The cloud ensemble		
Volume of Galaxy's star-forming disc	$V_{\rm TOT}$	$20\,\mathrm{kpc}^3$
Exponent of cloud mass-function	α	-1.75
Minimum cloud mass	$M_{\rm MIN}$	$100\,\mathrm{M}_\odot$
Maximum cloud mass	$M_{\rm MAX}$	$10^6\,\mathrm{M}_\odot$
Total mass of potential star-forming clouds in the Galaxy	$M_{\rm TOT}$	$3\times10^9\,\mathrm{M}_\odot$
The scaling relations		
Radius of notional '$\mathrm{M}_\odot$cloud'	$R_{\rm O}$	0.1 pc
Larson-type scaling exponent between cloud radius and cloud mass	β	0.5
Internal one-dimensional velocity dispersion inside a notional '$\mathrm{M}_\odot$cloud'	$\Delta v_{\rm O}$	$0.2\,\mathrm{km\,s^{-1}}$
Larson-type scaling exponent between internal velocity dispersion and cloud mass	γ	0.25
The fractal structure		
Maximum ratio of radii for clouds of comparable size	ϕ	2
The efficiency		
Overall efficiency of star formation following a collision	$\eta_{\rm SF}$	0.25
Overall mass of stars formed per massive star	$\Delta M_{\rm MSF}$	$100\,\mathrm{M}_\odot$
Maximum fractional impact parameter for star cluster formation	ψ	0.3

with $\alpha\simeq-1.75$, $M_{\rm MIN}\simeq100\,\mathrm{M}_\odot$ and $M_{\rm MAX}\simeq10^6\,\mathrm{M}_\odot$. The total mass of clouds is therefore

$$M_{\rm TOT}\simeq V_{\rm TOT}\int_{M=M_{\rm MIN}}^{M=M_{\rm MAX}}M\,\frac{\mathrm{d}n}{\mathrm{d}M}\,dM$$
$$\simeq\frac{V_{\rm TOT}K_{\rm O}\mathrm{M}_\odot^2}{(2+\alpha)}\times\left\{\left(\frac{M_{\rm MAX}}{\mathrm{M}_\odot}\right)^{(2+\alpha)}-\left(\frac{M_{\rm MIN}}{\mathrm{M}_\odot}\right)^{(2+\alpha)}\right\}\quad(A3)$$
$$\rightarrow 114\,V_{\rm TOT}\,K_{\rm O}\,\mathrm{M}_\odot^2.\quad(A4)$$

The total mass of clouds is estimated to be $M_{\rm TOT}\simeq3\times10^9\,\mathrm{M}_\odot$, so

$$K_{\rm O}\simeq\frac{(2+\alpha)\,M_{\rm TOT}}{V_{\rm TOT}\,\mathrm{M}_\odot^2}\times\left\{\left(\frac{M_{\rm MAX}}{\mathrm{M}_\odot}\right)^{(2+\alpha)}-\left(\frac{M_{\rm MIN}}{\mathrm{M}_\odot}\right)^{(2+\alpha)}\right\}^{-1}\quad(A5)$$
$$\rightarrow 1.32\times10^6\,\mathrm{kpc}^{-3}\,\mathrm{M}_\odot^{-1}.\quad(A6)$$

Assumption 2: The scaling relations. We assume that, within the star-forming disc, the radii and internal velocity dispersions of clouds subscribe to Larson-like relations,

$$R\simeq R_{\rm O}\left(\frac{M}{\mathrm{M}_\odot}\right)^{\beta},\quad(A7)$$

$$\Delta v\simeq\Delta v_{\rm O}\left(\frac{M}{\mathrm{M}_\odot}\right)^{\gamma},\quad(A8)$$

with $R_{\rm O}\simeq0.1$ pc, $\beta\simeq0.5$, $\Delta v_{\rm O}\simeq0.2\,\mathrm{km\,s^{-1}}$ and $\gamma\simeq0.25$.

Assumption 3: The fractal structure. We assume that the structure of the star-forming disc is fractal. The three-dimensional fractal dimension is given by

$$\mathcal{D}_3\simeq2+\alpha+\frac{1}{\beta}\quad(A9)$$
$$\rightarrow 2.25.\quad(A10)$$

Given a fractal structure, we infer that the majority of collisions involve clouds of comparable size (i.e. clouds on the same level of the fractal hierarchy), and that the bulk velocity of a cloud is some multiple – greater than one – of its internal velocity dispersion (basically, the bulk velocity of a cloud derives from the velocity dispersion on the next higher level of the fractal hierarchy). The requirement of comparable size is implemented as a requirement that the cloud radii differ by no more than a factor $\phi\simeq2$. Hence, the mean density of potential collision partners for a cloud of mass M is given by

$$\tilde{n}(M)\simeq\int_{M'=M\phi^{-1/\beta}}^{M'=M\phi^{+1/\beta}}\frac{\mathrm{d}n}{\mathrm{d}M}(M')\,dM'$$
$$\simeq\frac{(2+\alpha)M_{\rm TOT}}{(1+\alpha)V_{\rm TOT}\mathrm{M}_\odot}\left\{\phi^{(1+\alpha)/\beta}-\phi^{-(1+\alpha)/\beta}\right\}\times\left\{\left(\frac{M_{\rm MAX}}{\mathrm{M}_\odot}\right)^{(2+\alpha)}-\left(\frac{M_{\rm MIN}}{\mathrm{M}_\odot}\right)^{(2+\alpha)}\right\}^{-1}\times\left(\frac{M}{\mathrm{M}_\odot}\right)^{(1+\alpha)}\quad(A11)$$
$$\rightarrow 4.3\times10^6\,\mathrm{kpc}^{-3}\left(\frac{M}{\mathrm{M}_\odot}\right)^{-0.75}.\quad(A12)$$

Since the masses of a cloud's potential collision partners span a range $\phi^{2/\beta}$, the larger structure of which the cloud is part must be

larger by a similar factor. In a fractal distribution, it is the internal velocity dispersion of this larger structure that informs the relative bulk velocities of the constituent smaller clouds ('the cloud' and its most likely potential collision partners), so we set the mean bulk speed to

$$\Delta v_{+}(M) \simeq \phi^{2\gamma/\beta}\, \Delta v(M) \tag{A13}$$

$$\rightarrow 0.4\,\mathrm{km\,s^{-1}} \left(\frac{M}{\mathrm{M}_{\odot}}\right)^{0.25}. \tag{A14}$$

Assumption 4: The efficiency. On the basis of the simulations reported here, we assume that significant star formation (i.e. the formation of a large star cluster in which competitive accretion can deliver massive stars) requires a collision at impact parameter $b \lesssim \psi R$, with $\psi \simeq 0.3$. Hence, the effective cross-section for star formation is

$$\tilde{\sigma}(M) \simeq \pi \left\{ \psi R_{\mathrm{O}} \left(\frac{M}{\mathrm{M}_{\odot}}\right)^{\beta} \right\}^{2} \tag{A15}$$

$$\rightarrow 5 \times 10^{-9}\,\mathrm{kpc}^{2} \left(\frac{M}{\mathrm{M}_{\odot}}\right). \tag{A16}$$

On the basis of simulations including feedback from massive stars (Balfour, Whitworth & Hubber, in preparation), we assume that the efficiency of star formation following cloud/collisions is $\eta_{\mathrm{SF}} \simeq 0.25 \pm 0.05$ (i.e. higher than the 0.1 adopted in the simulations presented here), and that, with a standard initial mass function, a massive star is formed for every $\Delta M_{\mathrm{MSF}} \simeq 100\,\mathrm{M}_{\odot}$ converted into stars (of all masses). Hence, a collision involving two clouds of mass M produces, on average,

$$\mathcal{N}_{\mathrm{MSF}}(M) \simeq \begin{cases} \frac{2M\eta_{\mathrm{SF}}}{\Delta M_{\mathrm{MSF}}}, & \text{if} \geq 1, \\ 0, & \text{otherwise;} \end{cases} \tag{A17}$$

$$\rightarrow \begin{cases} 0.005 \left(\frac{M}{\mathrm{M}_{\odot}}\right), & \text{if} M \geq 200\,\mathrm{M}_{\odot}, \\ 0, & \text{if} M < 200\,\mathrm{M}_{\odot}. \end{cases} \tag{A18}$$

massive stars. For example, a collision between two $500\,\mathrm{M}_{\odot}$ clouds results in the formation of two or three massive stars. Collisions involving clouds with mass below $200\,\mathrm{M}_{\odot}$ do not produce massive stars, but might produce Taurus-like clusters with only lower mass stars.

With these assumptions, the rate of massive star formation due to cloud–cloud collisions is

$$\mathcal{R}_{\mathrm{MSF}} \simeq V_{\mathrm{TOT}} \times \int_{M_{\mathrm{MIN}}}^{M_{\mathrm{MAX}}} \frac{\tilde{n}(M)\tilde{\sigma}(M)\Delta v_{+}(M) 2^{1/2} \eta_{\mathrm{MSF}}(M)}{2} \frac{\mathrm{d}n}{\mathrm{d}M} dM. \tag{A19}$$

To recap, $\tilde{n}(M)$ is the mean density of potential collision partners, i.e. clouds having mass comparable to M [see equations (A11) and (A12)]; $\tilde{\sigma}(M)$ is the effective cross-section for collisions that trigger significant star formation [see equations (A15) and (A16)]; $\Delta v_{+}(M)$ is the bulk velocity of a cloud relative to its potential collision partners [see equations (A13) and (A14)], and the following $2^{1/2}$ takes account of the fact that the potential collision partners are moving too; $\eta_{\mathrm{MSF}}(M)$ is the efficiency of massive star formation [see equations (A17) and (A18)]; and the factor 2 in the denominator takes account of the fact that it takes two clouds to trigger one collision.

Substituting from equations (A11) through (A18), we obtain

$$\begin{aligned} \mathcal{R}_{\mathrm{MSF}} \simeq & \frac{2^{1/2}\pi(2+\alpha)^{2} M_{\mathrm{TOT}}^{2} R_{\mathrm{O}}^{2} v_{\mathrm{O}} \eta_{\mathrm{SF}} \phi^{2\gamma/\beta} \psi^{2}}{(1+\alpha)(3+2\alpha+2\beta+\gamma) V_{\mathrm{TOT}} \Delta M_{\mathrm{MSF}} \mathrm{M}_{\odot}} \\ & \times \left\{ \phi^{(1+\alpha)/\beta} - \phi^{-(1+\alpha)/\beta} \right\} \\ & \times \left\{ \left(\frac{M_{\mathrm{MAX}}}{\mathrm{M}_{\odot}}\right)^{(3+2\alpha+2\beta+\gamma)} - \left(\frac{M_{\mathrm{MIN}}}{\mathrm{M}_{\odot}}\right)^{(3+2\alpha+2\beta+\gamma)} \right\} \\ & \times \left\{ \left(\frac{M_{\mathrm{MAX}}}{\mathrm{M}_{\odot}}\right)^{(2+\alpha)} - \left(\frac{M_{\mathrm{MIN}}}{\mathrm{M}_{\odot}}\right)^{(2+\alpha)} \right\}^{-2} \end{aligned} \tag{A20}$$

$$\rightarrow 1.9 \times 10^{4}\,\mathrm{Myr}^{-1}. \tag{A21}$$

This estimate is highly uncertain because it depends on 13 parameters and/or exponents, none of which are particularly secure, and some of which have quite large uncertainties. In the Galaxy, massive stars are estimated to form at the rate of one per hundred years, i.e. $\mathcal{R}_{\mathrm{MSF}} \simeq 10^{4}\,\mathrm{Myr}^{-1}$. Therefore, it is possible that cloud/cloud collisions make a significant contribution to the rate of formation of massive stars, and they might even be the dominant contribution.

This paper has been typeset from a TEX/LATEX file prepared by the author.